Asian Journal of Chemistry; Vol. 32, No. 8 (2020), 1837-1848

ASIAN JOURNAL OF CHEMISTRY

https://doi.org/10.14233/ajchem.2020.22644

REVIEW

A Review on 2,6-Diformyl-4-methylphenol Derived Schiff Bases as Fluorescent Sensors

MRINAL SARKAR

Department of Chemistry, Derozio Memorial College, Kolkata-700136, India

Corresponding author: E-mail: msarkar81@gmail.com

Received: 20 January 2020; *Accepted*: 17 April 2020; *Published online*: 27 July 2020; AJC-19956

2,6-Diformyl-4-methylphenol fluorophore derived Schiff base sensors detect metal ions such as Zn^{2+}, Al^{3+}, Hg^{2+}, Cd^{2+}, Sn^{2+} and Cu^{2+} with high sensitivity and selectivity through changes in fluorescence intensity based on CHEF, ICT, FRET, ESIPT, C=N isomerization and PET mechanism. Several anions *viz*. HPO_4^{2-}, $H_2PO_4^-$, PO_4^{3-}, AsO_3^{3-}, $H_2AsO_4^-$, AsO_2^-, PPi (pyrophosphate), I^-, F^- and N_3^- were also detected through intermolecular hydrogen bonding (between sensor and anion) based on TICT, PET, CHEF, ESIPT and aggregation induced emission mechanism. Selectivity and sensitivity for these metal ions and anions were achieved by introducing various amines to core fluorophore 2,6-diformyl-4-methylphenol. Majority of these fluorescent sensors were Zn^{2+} ion selective. Due to the filled d^{10} electronic configuration of Zn^{2+} ion usually does not show deactivation of excited state *via* any electron or energy transfer mechanisms. Both solvent dependent and independent ten multi-ion selective sensors are found. This review will consolidate on 2,6-diformyl-4-methylphenol derived Schiff base fluorescent chemosensors.

Keywords: Cell imaging, Fluorescent chemosensor, 2,6-Diformyl-4-methylphenol, Selective multi-ion sensor.

INTRODUCTION

Organic compounds consist of a guest binding unit (receptor), a guest signaling unit (fluorophore/chromophore) and a mechanism for communication between the two units are called fluorescent chemosensors [1]. Guest signaling and guest binding moieties, either separated by a spacer or integrated into one unit. The development of chemosensors for ions (cation and anion) has received considerable attention due to their potential applications in environmental detection, molecular catalysis, and biological fluorescence imaging, *etc*. [2-6]. Several methods such as atomic absorption spectroscopy (AAS) [7], inductively coupled plasma mass spectroscopy (ICPMS) [8], inductively coupled plasma atomic emission spectroscopy (ICP-AES) [9], voltametry [10], UV-visible absorption spectroscopy, fluorescence spectroscopy and colorimetry [11,12] have been developed for detecting ions. Although AAS, ICPMS, ICP-AES methods are highly sensitive, they cannot be used for assays because they destroy the sample and also require expensive and technically demanding equipment. Fluorometric technique is the most promising tool alternative to the traditional analytical instruments, due to their high sensitivity, instantaneous response, non-destructive and cost-effectiveness [7,13]. Moreover, the distribution of guest ion within living cells can be mapped by the fluorescence imaging technique [14].

2,6-Diformyl-4-methylphenol derived Schiff bases have been used as fluorescent chemosensors due to their facile synthesis, stability in wide pH range, solubility in polar and mixed polar media, and good photophysical properties. These Schiff bases bind metal ions strongly through two N-atom of azomethine group (–CH=N–) with the phenolic OH group present at the centre of the binding cleft. To make these Schiff bases efficient anion binders, the H-bonding donor –NH, –OH (phenolic and hydroxyl) has been incorporated in the receptor unit. The majority of these fluorescent sensors are single-ion selective, while ten sensors are multi-ion responsive. Sensors that detect more than one ion simultaneously are described as multi-ion selective sensors. Multi-ion selective sensors are of great interest because they can differentiate and detect the analyte of interest in the presence of interfering ions and essentially important in the developing of multifaceted molecular logic gates, switching devices, *etc*. [15-18].

The solvent may affect the physico-chemical nature of the guest binding units of the sensors and thus, the fluorescence output and the selectivity toward analyte is highly influenced by the solvatochromic nature of the guest binding unit. The sensing of multiple analytes using a single sensor can be modulated in their selectivity to different ions with a change in the solvent. Sensors MI3, MI4 and MI5 show different recognition signals in different solvent media for sensing ions. The MI3 sensor displayed high selectivity and extremely high sensitivity for PO_4^{3-} and AsO_3^{3-} in 9:1 (v/v, HEPES buffer, pH 7.2) CH_3CN:H_2O mixed solvent and for Zn^{2+} and $H_2PO_4^-$ in 4:1 (v/v, 10 mM HEPES buffer, pH 7.2) CH_3OH:H_2O mixed solvent. MI4 (same as sensor-As3) chemosensor can sensitively and selectively recognize Zn^{2+} and Al^{3+} in the mixed solvent of C_2H_5OH:H_2O (v/v = 1:9, 0.1 M HEPES buffer, pH 7.4) and AsO_3^{3-} in the mixed solvent of DMSO:H_2O (v/v = 1:9, 1 mM HEPES buffer, pH 7.4). The MI5 sensor detects Al^{3+} in aqueous methanol (CH_3OH:H_2O = 1:1), its fluorescence was enhanced by 31-fold with a concomitant green emission at 525 nm. In contrast, when MI5 bound Zn^{2+} in DMSO, its fluorescence was enhanced by 19-fold accompanied by a yellow emission at 538 nm. Moreover, MI5 generates red color in the presence of I^- in THF with fluorescence enhancement by 37-fold at 636 nm.

2,6-Diformyl-4-methylphenol derived iminephenolato sensors detect metal ions (Zn^{2+}, Al^{3+}, Hg^{2+}, Cd^{2+}, Sn^{2+} and Cu^{2+}) with high sensitivity and selectivity through changes in fluorescence intensity based on CHEF (chelation enhanced fluorescence effect), ICT (intramolecular charge transfer), FRET (fluorescence resonance energy transfer), ESIPT (excited-state intra-molecular proton transfer), C=N isomerization and PET (photo-induced electron transfer) mechanism. Anions *viz*. HPO_4^{2-}, $H_2PO_4^-$, PO_4^{3-}, AsO_2^-, AsO_3^{3-}, $H_2AsO_4^-$, PPi (pyrophosphate), I^-, F^- and N_3^- anions were also detected through intermolecular hydrogen bonding (between sensor and anion) based on TICT (twisted intramolecular charge transfer), PET, CHEF, ESIPT and aggregation induced emission mechanisms [19-22]. Zn^{2+} complexes of the sensors (MI2, MI3, sensor-Zn4) recognize phosphate through the cation displacement approach and a cationic dinuclear Cu^{2+} complex (sensor-N_3) serves as a selective azide ion (N_3^-) sensor. Selectivity and sensitivity for these metal ions and anions were achieved by introducing various amines to core fluorophore 2,6-diformyl-4-methylphenol.

2,6-Diformyl-4-methylphenol derived Schiff base fluorescent sensors: They are made up of two components, (i) a guest binding unit (ionophore/receptor); and (ii) a guest signaling unit (fluorophore). In these sensors, the fluorophore and the guest binding units are covalently integrated within one unit. The photophysical responses of the sensors molecule occur by a possible excited state electron transfer process between the guest binding unit and guest signaling unit. The guest-recognition process takes place by the ionophore part that is then converted to a change in the fluorophore signal, brought about by perturbation of processes (photo-induced electron transfer, excited-state intramolecular proton transfer, *etc*.). The read-out of a fluorescent sensor is measured as a change in fluorescent intensity or intensity decay lifetime, or a shift in emission wavelength.

Cation sensing: In PET and ESIPT sensing, the fluorescence appears when the guest binding unit binds metal ion and, in the absence of metal ions, the fluorescence is quenched by PET and ESIPT (**Scheme-I**). However, a lone pair of electrons on N-atom of azomethine group (–CH=N–) of chemosensor is no longer available for PET due to complexation. Thus, the presence of metal ions leads to fluorescence enhancement.

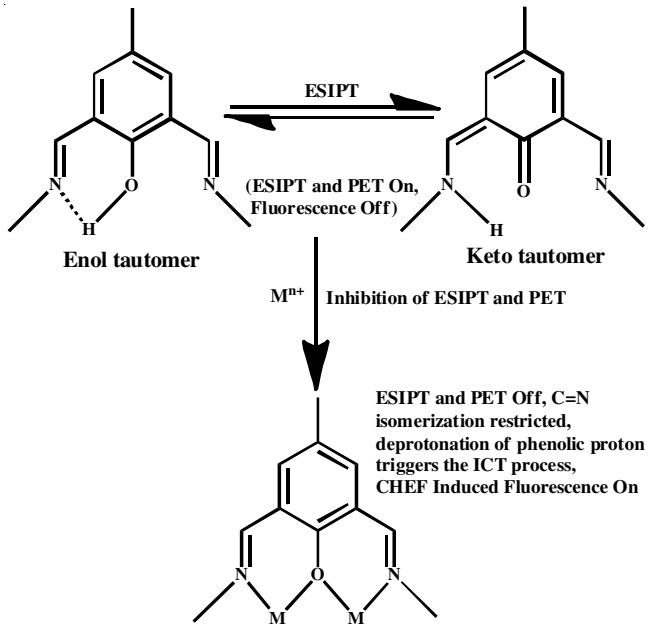

Scheme-I: Different mechanisms for fluorescent to detect cation

In addition, an enhancement of the fluorescence intensity was due to the formation of complex, which resulted in the selective CHEF effect. As a consequence of binding to metal ions, the restriction of C=N isomerization helps to enhance the fluorescence intensity. On binding with metal ions, the phenolic proton deprotonates, which triggers the ICT process and leads to the fluorescence enhancement. The coordination of metal ion imposes rigidity and as a consequence, decreases the non-radiative decay of the excited state.

FRET mechanism is observed with sensor-Al and sensor-Hg as both sensors are 2,6-diformyl-4-methylphenol-rhodamine conjugate. The excitation energy from the donor 2,6-diformyl-4-methylphenol is transferred to a nearby energy acceptor rhodamine unit. The intense fluorescence spectrum of 2,6-diformyl-4-methylphenol overlaps with the absorption spectrum of rhodamine unit.

Anion sensing: The weak fluorescence of the sensor is due to twisted intramolecular charge transfer (TICT) [19,20] and photoinduced electron transfer (PET) from lone pair of electrons on the N-atom of azomethine group (–CH=N–). In the presence of anion, there occurs hydrogen bonding between guest anion and -NH/-OH/-CH=N- group of the sensor. This intermolecular hydrogen bonding restricts the rotation of bonds adjacent to imine bonds (**Scheme-II**). Thus hydrogen bonding leads to inflexibility (planarity) in the structure. Planarity converts TICT to planar intramolecular charge transfer (PICT). PICT has higher emission intensity and in addition, inhibition of PET process (due to hydrogen bonding) enhance the emission

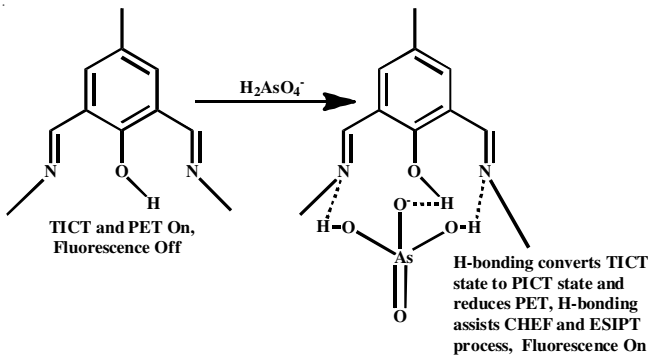

Scheme-II: Different mechanisms for fluorescent to detect anion

efficiency. The increment in fluorescence intensity also arises due to strong hydrogen bonding with guest oxo-anion and -NH/-OH/-CH=N- group of the sensor, which induces CHEF and ESIPT-emission with the enhancement of structural inflexibility.

Zn^{2+}-selective fluorescent sensors: Nine molecular fluorescent sensors have been used to detect Zn^{2+} in biological as well as in environmental systems. Being group 12 elements of the periodic table, Zn^{2+} and Cd^{2+} show cross-reactivity and the sensing of Zn^{2+} was interfered with Cd^{2+}. However, the nine sensors showed a negligible fluorescence enhancement in the presence of Cd^{2+}, thereby making it advantageous to distinguish between these two ions. $H_2PO_4^-$ has a strong affinity to Zn^{2+} and has been used in analytical chemistry for gravimetric estimation; thus the interaction of $H_2PO_4^-$ to [Sensor-Zn^{2+}] complex is found. Among the nine sensor-Zn^{2+} complexes, only the interaction of $H_2PO_4^-$ with sensor Zn4-Zn^{2+} complex had been studied.

Limits of detection (LODs) were in the range 10^{-7}-10^{-8} M. Fig. 1 shows the structures of Zn^{2+}-selective fluorescent sensors and its characteristic parameters are given in Table-1. The seven Zn^{2+}-sensitive fluorescent sensors (except sensor-Zn6 and Zn8) work within physiological pH values so that they can image living cells. The enhancements in fluorescence intensity of the nine sensors were observed with particularly Zn^{2+} ions due to filled d^{10} electronic configuration. The filled d^{10} electronic configuration usually does not show deactivation of excited state *via* any electron or energy transfer mechanisms [23].

Cations like Ca^{2+}, Mg^{2+}, Na^+ and K^+, which exist at high concentrations in living cells, do not enhance the fluorescence intensity even at a high concentration. These results are presumably due to the poor complexation of alkali metals or alkaline earth metals with the sensors. Among first-row transition metal cations, Cr, Mn, Fe, Co, Ni, and Cu quench the emission, owing to an electron or energy transfer between the metal cation and

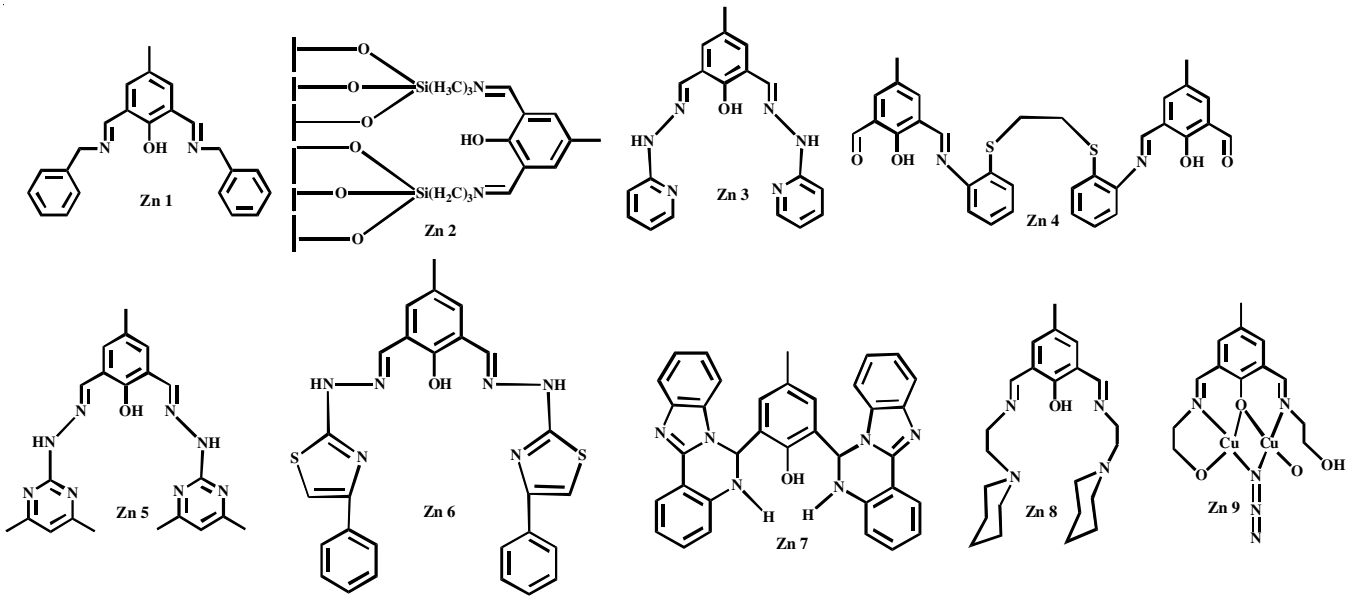

Fig. 1. Structure of some compounds used in Zn^{2+}-Selective fluorescent sensors

TABLE-1
CHARACTERISTICS OF Zn^{2+}-SELECTIVE FLUORESCENT SENSORS

Sensor used	Medium	$\lambda_{ex}/\lambda_{em}$ (nM)	Detection limit	Binding constant (M^{-1})	Mechanism	Ref.
Zn1	H_2O	400/484	–	1.5×10^4	PET, CHEF	[25]
Zn2	H_2O	430/500	6.54 μg L^{-1}	0.87×10^4	PET	[26]
Zn3	DMSO/H_2O (1:9)	350/476	–	3.2×10^7	PET	[27]
Zn4	CH_3OH/H_2O (2:1)	375/530	5.0×10^{-8}M	13.47×10^4	PET, ICT, CHEF	[28]
Zn5	DMSO/H_2O (1:9)	390/495	9.727×10^{-7}M	4.812×10^5	CHEF, PET, ESIPT	[29]
Zn6	DMSO/CH_3OH (3:7)	380/532	2.31×10^{-8} M	5.22×10^3	PET, C=N ISOMERIZATION	[30]
Zn7	DMSO/H_2O (1:9)	360/425	3.5×10^{-8} g L^{-1}	$3.1 (\pm 0.1) \times 10^7$	PET	[31]
Zn8	CH_3CN	395/455	–	2.5×10^4	CHEF, PET	[32]
Zn9	H_2O	385/454	–	5.0×10^4	CHEF, PET	[33]

fluorophore known as the fluorescence quenching mechanism [24].

Upon gradual addition of Zn^{2+} to a 100 mM HEPES buffer solution (pH = 7.4) of sensor-Zn1 (λ_{ex} = 400 nm), the fluorescence intensity maximum at 530 nm is changed and a new peak of emission band centered at 484 nm appears by six fold fluorescence enhancement (Φ = 0.040 to Φ = 0.250). The binding constant was 1.5×10^4 M^{-1} and 1:3 sensor-Zn binding mode. Sensor-Zn1 exhibited ratiometric signaling as I_{484}/I_{530} increases with the gradual increase in the concentration of Zn^{2+} [25].

Aqueous suspension of sensor-Zn2 selectively detects Zn^{2+} ions in H_2O. Upon the incremental addition of Zn^{2+} (5 µM-1.4 mM, an excitation wavelength of 430 nm), the fluorescence intensity increases, fluorescence maximum shifted from 530 to 500 nm and the emission peak becomes broad. The broad band was due to the inhomogeneous binding of Zn^{2+} with the chromophore units of the sensor. Sensor-Zn2 shows three-fold fluorescence enhancement (Φ = 0.128 to Φ = 0.314) with binding constant 0.87×10^4 M^{-1} and limit of detection 6.54 µg L^{-1} [26].

Upon the addition of 10 µM Zn^{2+} to sensor-Zn3 (10 µM), the sensor showed 'naked-eye' detection by a colour change from colourless to yellow colour. In fluorescence spectrum, (50 mM HEPES buffer, DMSO:H_2O = 1:9, v/v, pH = 7.2), Zn^{2+} addition created 14-fold fluorescence enhancement (Φ = 0.020 to Φ = 0.280) at 476 nm while excitation wavelength was 350 nm. The binding of sensor-Zn3 to Zn^{2+} shows 1:1 stoichiometry with a binding constant 3.2×10^7 M^{-1}. The fluorescence intensity was unaffected between pH 5.5 and 9, which meets the physiological condition. EDTA was used to check the chemical reversible binding behaviour of sensor-Zn3 to Zn^{2+} [27].

Sensor-Zn4 detects Zn^{2+} ion in methanol-water mixture (v/v, 2:1, pH-7.2, 10 mM HEPES buffer). In the presence of Zn^{2+}, sensor-Zn4 shows the colour change from colorless to yellow. In fluorescence studies, without the addition of Zn^{2+}, a weak emission (Φ = 0.0012, λ_{ex} = 375 nm) observed at 575 nm. Upon the incremental addition of Zn^{2+} into the sensor-Zn4, a new band at 530 nm observed with 43 fold fluorescence enhancements (Φ = 0.052). The limit of detection is 5.0×10^{-8} M and sensor-Zn4 with Zn^{2+} shows 1:1 binding mode. The association constant was found to be 13.47×10^4 M^{-1}. Upon the addition of $H_2PO_4^-$, the colour of [Zn-sensor] complex changed from yellow to colourless. In the fluorescence titration of [Zn-sensor] complex with $H_2PO_4^-$, the band intensity at 530 nm for [Zn-sensor] complex was decreased due to the formation of $[Zn(H_2PO_4)_2]$. This observation indicates that $H_2PO_4^-$ selectively dechelates the sensor from the [Zn-sensor] complex [28].

Sensor-Zn5 exhibits a selective fluorescent detection (λ_{ex} = 390 nm) of Zn^{2+} ions in HEPES buffer solution (50 µM; DMSO:H_2O = 1:9, v/v, pH 7.2). Sensor-Zn5 forms 1:1 complex with Zn^{2+} and the association constant is 4.812×10^5 M^{-1}. The fluorescence intensity of sensor-Zn5 at 495 nm remained unaffected between pH 5.5 and 8.2, which meets the physiological condition. The reversible binding of sensor-Zn5 with Zn^{2+} was checked by EDTA [29].

The weak fluorescence intensity of sensor-Zn6 in DMSO:CH_3OH (3:7, v/v) at 520 nm (excitation wavelength 380 nm) was enhanced in the presence of Zn^{2+} ions and shifted to 532 nm. The association constant and detection limit were calculated to be 5.22×10^3 M^{-1} and 2.31×10^{-8} M, respectively. Sensor-Zn6 binds to Zn^{2+} ions in 1:2 ratios. Zn^{2+} ions ratiometrically displace Cd^{2+} ions from sensor Zn6-Cd^{2+} complex and hence sensor-Zn6 shows excellent selectivity towards *in situ* detection of Zn^{2+} ions in the presence of Cd^{2+}. Disodium salt of EDTA was used to check the reversible binding behaviour of sensor-Zn6 to Zn^{2+} [30].

Sensor-Zn7 selectively and sensitively detects Zn^{2+} in 50 mM HEPES buffer (DMSO:H_2O = 1:9, v/v, pH = 7.2) with a 1:2 (sensor:Zn^{2+}) binding stoichiometry. The emission peak of sensor-Zn7 (λ_{ex} = 360 nm) at 425 nm, undergoes 12-fold enhancement (Φ = 0.019 to Φ = 0.237) upon complexation with Zn^{2+}. The binding constant for *in situ* formed Zn^{2+} complex and the limit of detection were 3.1 (± 0.1) × 10^7 mol^{-1} L and 3.5×10^{-8} g L^{-1}, respectively. The enhancement of fluorescence intensity of sensor-Zn7 towards Zn^{2+} was almost stable around pH = 6.0-9.0, which meets the physiological condition [31].

Emission intensity at 512 nm of sensor-Zn8 (0.2 mM) in CH_3CN upon excitation at 395 nm was decreased along with the emergence of a new emission at 455 nm (97 fold enhancement) while Zn^{2+} (0-0.8 mM) is incrementally added to the sensor. Job's plot, mass spectrum and crystal structure confirmed that the sensor form dinuclear complex with Zn^{2+} (sensor:Zn = 1:2). Based on fluorescence titration, the binding constant value has been determined to be 2.5×10^4 M^{-1} [32].

Sensor-Zn9 (50 µM) excited at 385 nm in 100 mM HEPES buffer exhibits an emission at 434 nm, which underwent a red shift to 454 nm and emission intensity increased by 19-fold upon incremental addition of Zn^{2+} ions (0-1 mM). A Job plot and ESI mass spectrum suggest the formation of 1:2 (sensor:Zn^{2+}) complex with Zn^{2+}. Based on fluorescence titration, the binding constant was evaluated to be 5.0×10^4 M^{-1}. The emission spectrum of the sensor-Zn9 in the presence or absence of Zn^{2+} was almost unaltered between pH 5.5 and 9, which meets physiological pH [33].

Multi-ion selective fluorescent sensors: Fig. 2 shows the structures of multi-ion selective fluorescent sensors and their characteristic parameters are given in Table-2. In naked-eye study, sensor-MI1 shows a highly selective colour change from orange-red to blood-red upon the addition of Al^{3+} ions and color change from orange-red to yellow upon the addition of Zn^{2+}. Sensor-MI1 formed a complex with Zn^{2+} and Al^{3+} in 2:1 ligand to metal stoichiometry. The fluorescence titration of sensor-MI1 was performed in the presence of cations Cr^{3+}, Fe^{3+}, Co^{2+}, Ni^{2+}, Cu^{2+}, Zn^{2+}, Cd^{2+}, Hg^{2+}, Pb^{2+}, Al^{3+}, Na^+, Mg^{2+}, K^+, Ba^{2+} in 1 mM HEPES buffer solution (DMSO:H_2O = 3:2, v/v, pH7.4) at 372 nm excitation wavelength. However, the fluorescence enhancement was found for Al^{3+} at 580 nm by 750-fold and for Zn^{2+} at 505 nm by 365-fold. From the fluorescence titrations, the association constants of sensor-MI1 for Zn^{2+} and Al^{3+} were evaluated 3×10^3 and 2.5×10^3 M^{-1} L, respectively.

The transmetallation of one complex with second metal ion was observed because of close association constants of

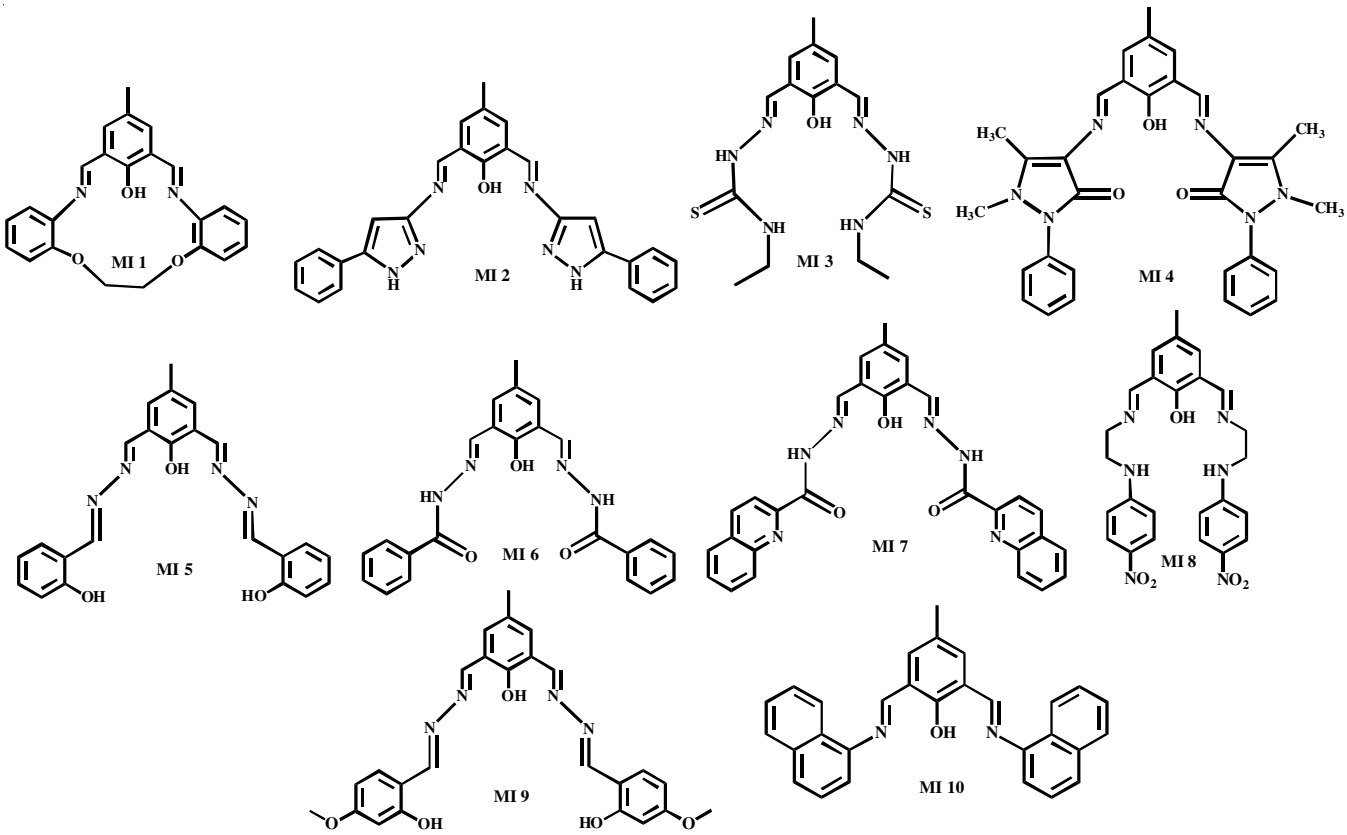

Fig. 2. Structure of compounds used in multi-ion selective fluorescent sensors

TABLE-2
CHARACTERISTICS OF MULTI-ION-SELECTIVE FLUORESCENT SENSORS

Sensor used	Medium	$\lambda_{ex}/\lambda_{em}$ (nM)	Detection limit	Binding constant (M^{-1})	Mechanism	Ref.
MI1	DMSO/H_2O (3:2)	372/580 (Al^{3+}), 372/505 (Zn^{2+})	1.2 μM (Al^{3+}), 21 nM (Zn^{2+})	2.5×10^3 (Al^{3+}), 3×10^3 (Zn^{2+})	ESIPT, CHEF	[34]
MI2	DMSO	440/520 (Zn^{2+}), 440/595 (HPO_4^{2-})	27.80 nM (Zn^{2+}), 3.12×10^{-7} M (HPO_4^{2-})	–	CHEF	[35]
MI3	MeOH/H_2O (4:1)	348/492 (Zn^{2+})	0.59 nM (Zn^{2+}), 26 μM ($H_2PO_4^-$)	2.5×10^6 (Zn^{2+}) –	CHEF, ESIPT, ICT	[36]
MI3	CH_3CN/H_2O (9:1)	458/560 (PO_4^{3-}), 458/560 (AsO_3^{3-})	34 nM (PO_4^{3-}), 15 nM (AsO_3^{3-})	5.2×10^4 (PO_4^{3-}), 1.0×10^5 (AsO_3^{3-})	ESIPT	[37]
MI4	C_2H_5OH/H_2O (1:4)	385/520 (Zn^{2+}), 385/490 (Al^{3+})	5.7×10^{-7}M (Zn^{2+}), 4.6×10^{-8} M (Al^{3+})	$(4.9\pm0.2) \times 10^4$ (Zn^{2+}), $(3\pm0.1) \times 10^5$ (Al^{3+})	CHEF	[38]
MI5	CH_3OH/H_2O (1:1, Al^{3+}), DMSO (Zn^{2+}), THF (I^-)	390/525 (Al^{3+}), 390/538 (Zn^{2+}), 390/636 (I^-)	$6.8 \times 10^{?8}$ M (Al^{3+}), 5.7×10^{-8} (Zn^{2+}), $1.2 \times 10^{?7}$ M ($I^?$)	5.2×10^4 (Al^{3+}), 7.9×10^4 (Zn^{2+}), 3.6×10^4 (I^-)	C=N isomerization, ESIPT, CHEF, ICT	[39]
MI6	CH_3CN/0.02 M HEPES buffer (2:8)	370/493 (Cu^{2+}), 370/497 (Zn^{2+}), 370/545 (PPi)	0.272 nM (Cu^{2+}), 0.252 nM (Zn^{2+}), 7.16×10^{-9}M (PPi)	1.87×10^6 (Cu^{2+}), 2.68×10^5 (Zn^{2+}), 1.87×10^6 (PPi)	PET	[23]
MI7	5 mM HEPES buffer containing 0.33% of DMSO for Al^{3+} and Zn^{2+}. CH_3CN containing 0.33% DMSO for F^-	450/500 (Al^{3+}), 450/550 (Zn^{2+}), 450/575 (F^-)	32 ppb (Al^{3+}), 35 ppb (Zn^{2+}), 40 ppb (F^-)	1.07×10^5 $M^{?2}$ (Al^{3+}), 1.75×10^5 $M^{?2}$ (Zn^{2+})	ICT, CHEF	[40]
MI8	CH_3OH/H_2O (8:2)	370/486 (Al^{3+}), 370/534 (PPi)	7.55 μM (Al^{3+}), 3.34 μM (PPi)	$(5.29 \pm 1.11) \times 10^4$ (Al^{3+}), $(1.34 \pm 0.81) \times 10^3$ (PPi)	ESIPT, C=N isomerization	[41]
MI9	DMSO/H_2O (9:1)	482/545 (Zn^{2+}), 482/560 (Cd^{2+}), 530/630 (I^-)	2.7×10^{-9}M (Zn^{2+}), 6.6×10^{-9}M (Cd^{2+}), 5×10^{-9}M (I^-)	2.7×10^4 (Zn^{2+}), 0.96×10^4 (Cd^{2+}), 5.2×10^4 (I^-)	CHEF, ESIPT	[42]
MI10	CH_3CN (Sn^{2+}), CH_3OH/H_2O (1:1, Al^{3+})	330/420, 582 (Sn^{2+}), 330/490 and 375/501 (Al^{3+})	25.7 nM (Sn^{2+}), – (Al^{3+})	~3.4×10^5 (Sn^{2+}) – (Al^{3+})	CHEF, ESIPT	[43]

two metal ions Zn^{2+} and Al^{3+} with sensor-MI1. Upon the addition of metal ion to sensor-MI1, the highest emissivity was observed at pH 9 [34].

The weak emission intensity of sensor-MI2 in DMSO at 520 nm (excitation wavelength 440 nm) was enhanced by about 11-fold upon incremental addition of Zn^{2+} ions (0-15 μM). The maximum emission was found at a 2:1 ratio (sensor:Zn^{2+}) and pH 7. Based on the fluorescence enhancement, the detection limit was calculated to be 27.8 nM. In the presence of Zn^{2+} ions, the fluorescence enhancement was due to the formation of a dinuclear zinc complex of an in situ formed macrocyclic ligand. In the fluorescence titration of sensor-zinc complex (25 μM) in DMSO by HPO_4^{2-} ions (0-75 μM), the emission band at 520 nm was quenched and a new band appeared at 595 nm. The enhancement of fluorescence was by two-fold upon the addition of HPO_4^{2-} anions to zinc-complex, Zn^{2+} ions come out of the macrocyclic ligand and form $Zn(HPO_4)$ species. As a result, macrocyclic ligand breaks and original sensor-MI2 is formed. Due to the formation of sensor-MI2, an emission band at 595 nm was found. The detection limit of HPO_4^{2-} anion was 3.12×10^{-7} M [35].

Sensor-MI3 (in aqueous CH_3OH): In the naked eye study, sensor-MI3 changes colour from colorless to yellow in the presence of Zn^{2+} ions. The weak emission of sensor-MI3 (Φ = 0.008) in 10 mM HEPES buffer solution ($CH_3OH:H_2O$ = 4:1, v/v, pH 7.2) at 428 nm (excitation wavelength 348 nm) is enhanced (0.272) by 34-fold at 492 nm upon incremental addition of Zn^{2+} ions. The limit of detection and the binding constant were determined to be 0.59 nM and 2.5×10^6, respectively. In the presence of Zn^{2+} ions, the sensor-MI3 shows maximum emission at pH 7, which meets biological pH. Upon incremental addition of $H_2PO_4^-$ to sensor-zinc complex, emission intensity at 492 nm decreases due to the formation of [$Zn(H_2PO_4)$ + Na + H] and [sensor-MI3 + Zn + $H_2PO_4^-$], *etc*. The detection limit for $H_2PO_4^-$ was found to be 26 μM [36].

Sensor-MI3 (in aqueous CH_3CN): Excitation of the sensor-MI3 at 458 nm, exhibits feeble emission at 555 nm (Φ = 0.009) in $CH_3CN:H_2O$ (9:1, v/v, HEPES buffer, pH 7.2). The fluorescence enhancement at 560 nm is observed upon addition of PO_4^{3-} (Φ = 0.279, 31-fold) and AsO_3^{3-} (Φ = 0.315, 35-fold). Based on fluorometric titration, the binding constant for AsO_3^{3-} and PO_4^{3-} were found to be 1.0×10^5 M^{-1} and 5.2×10^4 M^{-1}, respectively. The detection limit for PO_4^{3-} and AsO_3^{3-} were calculated to be 34 nM and 15 nM, respectively. Other anions do not interfere in selective detection of PO_4^{3-} and AsO_3^{3-} by sensor-MI3. However, PO_4^{3-}/AsO_3^{3-} interferes ions with each other. Based on absorption spectroscopy, Job's plot, mass spectroscopy and ^1H NMR spectroscopy support the 1:1 stoichiometry of anions with sensor-MI3 [37].

Upon excitation at 385 nm, sensor-MI4 (20 μM) in 0.1 M HEPES buffer solution ($C_2H_5OH:H_2O$ = 1:4, v/v, pH 7.4) exhibits a fluorescence emission at 575 nm (Φ = 0.01). The fluorescence enhancement is observed for Zn^{2+} (Φ = 0.12) at 520 nm by 12 fold and for Al^{3+} (Φ = 0.23) at 490 nm by 23-fold. The X-ray crystal structure and Job's plots support the stoichiometries of the sensor-Zn^{2+} and sensor-Al^{3+} complexes to be 1:1. The association constants for the sensor-metal ion complexes were obtained from the slopes of the plots. These values were $(4.9 \pm 0.2) \times 10^4$ M^{-1} and $(3.0 \pm 0.1) \times 10^5$ M^{-1} for sensor-Zn^{2+} and sensor-Al^{3+}, respectively. The selective recognition of Zn^{2+} and Al^{3+} were at concentrations as low as 5.7×10^{-7} M and 4.6×10^{-8} M, respectively. The sensor-Zn^{2+} complex detects Al^{3+} in a greener way (0.1 M HEPES buffer, $C_2H_5OH:H_2O$ = 1:9, v/v, pH 7.4) by the displacement mechanism. Sensor-Zn^{2+} complex detects Al^{3+} at a lower detection limit (2.5×10^{-9} M) than that of the free sensor. Sensor-MI4 senses Zn^{2+} and Al^{3+} from pH 6.0 to 11.0 which meets the physiological pH [38].

Upon excitation at 390 nm, sensor-MI5 showed emission at 636 nm in aqueous methanol, DMSO and THF. The emission intensity of sensor-MI5 (Φ = 0.014) in 0.1 M HEPES buffered aqueous methanol ($CH_3OH:H_2O$ = 1:1, v/v, pH 7.4) increases at 525 nm (Φ = 0.430) upon gradual addition of Al^{3+} ions (0- 50 μM). Very weak emission of sensor-MI5 (Φ = 0.018) in DMSO was enhanced significantly in a ratiometric manner upon the addition of Zn^{2+} (Φ = 0.350) and a new emission band at 538 nm. Sensor-MI5 can detect I^- by the naked eye, as in the presence of I^- in THF, it exhibits remarkable red colour. The fluorescence titration of sensor-MI5 with I^- in THF, the weak emission intensity of the sensor-MI5 (Φ = 0.011) was enhanced upon the addition of I^- (Φ = 0.41). Job's plot and mass spectrum support 1:1 binding interaction between sensor-MI5 and Al^{3+}, Zn^{2+}, I^- respectively. The sensor-MI5 detects I^-, Al^{3+} and Zn^{2+} at concentrations as low as 1.2×10^{-7} M, 6.8×10^{-8} M and 5.7×10^{-8} M, respectively. However, binding constants for these ions are 3.6×10^4 M^{-1}, 5.2×10^4 M^{-1} and 7.9×10^4 M^{-1} for I^-, Al^{3+} and Zn^{2+}, respectively [39].

Moderate emission of **sensor-MI6** in CH_3CN/0.02 M HEPES (pH 7.3) at 493 nm was quenched by 9-fold upon the gradual addition of increasing amounts of aqueous Cu^{2+} solutions (0-5.5 μM). In contrast, in the presence of Zn^{2+} ions, the emission band shifted to a little longer wavelength at 497 nm and was enhanced by 4.1 fold. Based on fluorescence titration, the stoichiometry plot analysis showed a 1:2 and 1:1 stoichiometry between sensor-MI6 and Cu^{2+} and Zn^{2+} ions, respectively and the association constants were 1.87×10^6 M^{-1} for Cu^{2+} and 2.68×10^5 M^{-1} for Zn^{2+}. The stoichiometries of the complexes were also supported by XRD and ESI-MS analysis. In the naked eye study, sensor-MI6 shows a colour change from colourless to yellowish-green in the presence of Cu^{2+} ions. The reversible binding nature between sensor-MI6 and Zn^{2+} ions and Cu^{2+} ions was checked by EDTA titration. In 0.02 M HEPES buffer (pH 7.8), sensor-MI6-Zn^{2+} complex exhibits a strong emission at 497 nm, which (excitation wavelength 370 nm) is shifted at 545 nm and quenched by 4.5-fold after the addition of PPi (pyrophosphate). Based on fluorescence titration, detection limits were calculated to be 0.272 nM for Cu^{2+}, 0.252 nM for Zn^{2+} and 7.16×10^{-9} M for PPi ions [23].

Upon excitation at 450 nm, sensor-MI7 (25 μM, Φ = 0.002) in a 5 mM HEPES buffer containing 0.33% of DMSO exhibited weak emission at 520 nm. Sensor-MI7 displayed a remarkable increase in fluorescence intensity at 500 nm for Al^{3+} (Φ = 0.42) and at 550 nm for Zn^{2+} (Φ = 0.54). The 1:2 stoichiometries between the sensor and for both Al^{3+} and Zn^{2+} were validated by Job's plot. The association constants 1.07×10^5 M^{-2} for

Al^{3+} and 1.75×10^5 M^{-2} for Zn^{2+} were derived from the B-H plot. The detection limits for Al^{3+} and Zn^{2+} were found to be 32 ppb and 35 ppb, respectively. Upon incremental addition of F^- anions to sensor-MI7 ($\Phi = 0.002$, 25 μM) in an acetonitrile medium containing 0.33% DMSO displayed emission at 575 nm ($\Phi = 0.40$). The 1:1 stoichiometry of the ensemble between sensor and F^- was obtained from Job's plot. The detection limit of the sensor for F^- was 40 ppb. Due to the non-toxic nature, the sensor can also detect intracellular Al^{3+} and Zn^{2+} ions [40].

The solution of sensor-MI8 in CH_3OH:H_2O (8:2; v/v) in HEPES buffer at pH 7.2 exhibited very weak fluorescence ($\Phi = 0.002$) at 520 nm, attributed to the ESIPT from the phenolic –OH to the azomethine-N atom (–CH=N–) and the C=N isomerization. The addition of Al^{3+} or PPi ions to the sensor solution (20 μM) resulted in the fluorescence enhancements at 486 ($\Phi = 0.011$) and 534 nm (0.003), respectively, at an excitation wavelength of 370 nm. The fluorescence response in the case of Al^{3+} was ascribed to the complexation with Al^{3+}, ESIPT and C=N isomerization blocked. In the case of PPi, H-bonding between sensor-MI8 and PPi gives a rigid structure, as a consequence, ESIPT and C=N isomerization are blocked. Based on the fluorescence titration, the chemosensor showed binding constant and detection limit of $(5.29 \pm 1.11) \times 10^4$ M^{-1} and 7.55 μM for the Al^{3+} ions, respectively. For PPi anions, the binding constant and detection limit were found to be $(1.34 \pm 0.81) \times 10^3$ M^{-1} and 3.34 μM, respectively. The stoichiometry between the sensor and both the ions were evaluated to be 1:1. The selective and reversible binding nature of the sensor towards Al^{3+} and PPi was also verified. In addition, the sensor was employed for the intracellular detection of Al^{3+} and PPi ions, thus, exhibited the biological applicability [41].

Upon excitation at 482 nm, the sensor-MI9 (50 μM) in DMSO:H_2O (9:1, v/v) HEPES-buffer (pH 7.2) medium remains silent. However, upon the gradual incremental addition of Zn^{2+} (5 μM) or Cd^{2+} (5 μM) to sensor-MI9 (50 μM) has rendered a gradual enhancement of the fluorescence intensity. The solution of Zn^{2+} and sensor-MI9 showed emission at 545 nm along with 90-fold enhancement in the fluorescence intensity. On the other hand, the solution of Cd^{2+} and sensor-MI9 exhibited emission at 560 nm. For both metal ions, the excitation wavelength was the same (482 nm). The enhancement in the fluorescence intensity on the interaction of sensor-MI9 with Zn^{2+} and Cd^{2+} was due to the CHEF through N,O donor centres. Upon excitation at 530 nm, the sensor-MI9 (50 μM) in THF (HEPES buffer, pH 7.2) solution did not exhibit any significant emission. However, upon addition of I^- (5 μM), sensor-MI9 showed emission at 630 nm along with 600-fold fluorescence enhancement compare to the free sensor. Hence, the enhancement in the fluorescence intensity was due to the ESIPT process. Job′s plot, mass spectrum and binding constant value (B-H plot) support 1:1 binding interaction between sensor-MI9 and Zn^{2+}, Cd^{2+} and I^-, respectively. The sensor-MI9 detects Zn^{2+}, Cd^{2+} and I^- at concentrations as low as 2.7×10^{-9} M, 6.6×10^{-9} M and 5×10^{-9} M, respectively. However, binding constants for these ions were 2.7×10^4 M^{-1}, 0.96×10^4 M^{-1} and 5.2×10^4 M^{-1} for Zn^{2+}, Cd^{2+} and I^-, respectively [42].

Weak monomer emission intensity at 420 nm of the sensor-MI10 (20 μM) in CH_3CN upon excitation at 330 nm increases along with the emergence of a new emission at 582 nm, while Sn^{2+} (0-50 μM) was incrementally added to the sensor. The new emission arises due to the formation of an intramolecular excimer between the naphthalene units of the sensor-MI10. Interestingly, when the concentration of Sn^{2+} exceeds 50 μM, the monomer emission at 420 nm decreases. However, the excimer emission at 582 nm increases. Based on the fluorescence titration data, the binding constant and detection limit were determined to be ~3.4×10^5 and 25.7 nM. The Job′s plot supports 1:1 stoichiometry between Sn^{2+} and sensor-MI10. Sensor-MI10 also detects Al^{3+} ion in methanol-water mixture (1:1, v/v). Upon excitation at 330 nm, sensor-MI10 exhibits a broad emission peak centred at 490 nm in the presence of Al^{3+}. However, excitation at a different wavelength (375 nm), the [sensor-Al^{3+}] complex shows a sharp emission peak at 501 nm [43].

Cu^{2+}-selective fluorescent sensors: Fig. 3 shows the structures of Cu^{2+}-selective fluorescent sensors and their characteristic parameters are given in Table-3. Upon the addition of Cu^{2+} ions, a solution of sensor-Cu1 turned from reddish to colourless. So, Cu^{2+} ions can be detected by naked eye. When a solution of sensor-Cu1 (10 μM) in 1 mM HEPES buffer (CH_3CN:H_2O=1:4, v/v, pH 7.3) was excited at 380 nm, it exhibits two distinct emissions at 441 and 544 nm, respectively. Upon gradual addition of increasing amounts of Cu^{2+} ions to the solution of sensor-Cu1, the fluorescence intensity at 544 nm was increased by near about 600-fold and simultaneously fluorescence intensity at 441 nm was decreased. The fluorescence intensity ratio of emission at 441 nm to that at 544 nm (I_{441}/I_{544}) decreases with the increase in amounts of Cu^{2+} ions. The plot of (I_{441}/I_{544}) *versus* concentration of Cu^{2+} suggested a 1:2 stoichiometry (sensor: Cu^{2+}), which was also established by ESI-MS and Job′s plot. The association constant and the detection limit were evaluated to be 9.13×10^8 M^{-1} and 2.1 ppb, respectively. The non-cytotoxic sensor-Cu1 can detect intracellular Cu^{2+} by fluorescence microscopy [44].

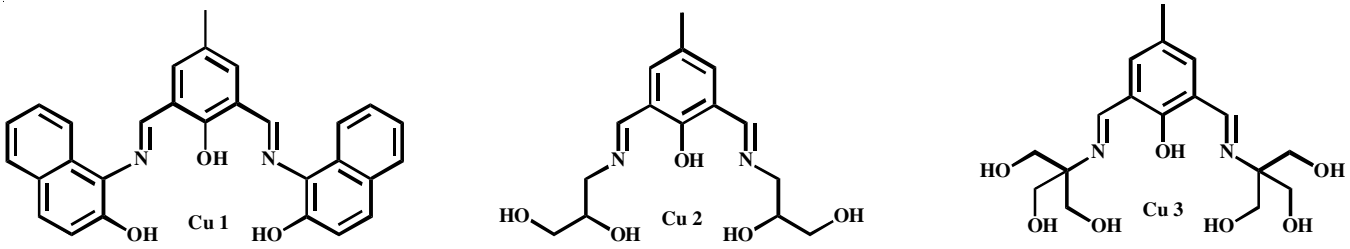

Fig. 3. Cu^{2+}-selective fluorescent sensors

TABLE-3
CHARACTERISTICS OF Cu^{2+}- SELECTIVE FLUORESCENT SENSORS

Sensor used	Medium	$\lambda_{ex}/\lambda_{em}$ (nM)	Detection limit	Binding constant (M^{-1})	Mechanism	Ref.
Cu1	CH_3CN/H_2O (1:4)	380/544	2.1 ppb	9.13×10^8	CHEF, ICT	[44]
Cu2	H_2O	434/510	11.2 nM	4.99×10^{11} M^{-2}	PET	[45]
Cu3	H_2O	Independent/505	1 ppm	1×10^2 M^{-2} [(sensor-Cu3)$_2Cu^{II}$] 4×10^4 M^{-2} [(sensor-Cu3)Cu_2^{II}]	–	[46]

Sensor-Cu2 changes colour from yellow to sky blue on the addition of Cu^{2+} ions and enables naked-eye detection. When the sensor-Cu2 in 25 mM tris-buffer at pH 7.4 excited at 434 nm, it exhibits a strong emission at 510 nm ($\Phi = 0.248$). The fluorescence intensity of sensor-Cu2 (5 μM) at 510 nm decreases gradually ($\Phi = 0.035$) upon the gradual addition of increasing amounts of Cu^{2+} ions (0 – 50μM). Based on the fluorescence titration data, the binding constant and detection limit were estimated to be 4.99×10^{11} M^{-2} and 11.2 nM, respectively. The reversible binding between sensor-Cu2 and Cu^{2+} was checked by EDTA. Sensor-Cu2 can detect intracellular Cu^{2+} ions through fluorescence microscopy [45].

Excitation wavelength-independent, the moderate fluorescence intensity of sensor-Cu3 in tris-buffer (pH 7.5) at 505 nm ($\Phi = 0.37$) continues to decrease upon the gradual addition of increasing amounts of Cu^{2+} ions and becomes quenched upon addition of 2 equiv. of Cu^{2+}. The yellow colour of sensor-Cu3 (10 μM) in tris-buffer (pH 7.5) solution becomes almost colourless upon the addition of Cu^{2+} ions (20 μM) and enables naked-eye detection. Job′s plot based on absorption at 375 nm indicates that the binding stoichiometry between sensor-Cu3 and Cu^{2+} are two types 1:2 and 2:1. Based on the absorbance of sensor-Cu3 at 430 nm, the binding constants for the two complexes [(sensor-Cu3)$_2Cu^{II}$] and [(sensor-Cu3)Cu_2^{II}] were evaluated to be 1×10^2 and 4×10^4 M^{-2}, respectively. Sensor-Cu3 can detect Cu^{2+} upto detection level 20 ppm by the naked eye and 1 ppm by the use of spectrofluorimeter. The sensor-Cu3 can also detect intracellular Cu^{2+} ions by fluorescence microscopy [46].

Arsenicals-selective fluorescent sensors: Fig. 4 shows the structures of arsenicals-selective fluorescent sensors and their characteristic parameters are given in Table-4. In 0.1 M HEPES buffer (C_2H_5OH:H_2O = 1:99, v/v, pH 7.4), the weak emission intensity ($\Phi = 0.015$, $\lambda_{ex} = 440$ nm) of sensor-As1 (10 μM) at 532 nm was enhanced by about 19-fold ($\Phi = 0.17$) upon gradual addition of increasing amounts of $H_2AsO_4^-$ anions (0-8 μM). The stoichiometry of adduct between sensor-As1 and $H_2AsO_4^-$ was 1:1, which is supported by Job′s plot and mass spectrum. Based on fluorescence titration, the association constant and limit of detection were evaluated to be 1.35×10^6 M^{-1} and 0.001 μM. Sensor-As1 can detect intracellular arsenate. Sensor-As1 appended merrifield polymer (chloromethyl polystyrene) can remove $H_2AsO_4^-$ from contaminated water [47].

Upon excitation at 340 nm, sensor-As2 in 10 mM HEPES buffer in H_2O (pH 7.2, μ = 0.05 M, NaCl) exhibits a weak emission ($\Phi = 0.031$) at 460 nm. The emission intensity at 460 nm was enhanced by two-fold ($\Phi = 0.055$) after incremental addition of $H_2AsO_4^-$ anions and red shifted to 476 nm with five-fold enhancement ($\Phi = 0.078$) upon addition of AsO_2^- anions. Based on fluorescence titration, the limits of detection were evaluated to be 0.23 μM for $H_2AsO_4^-$ and 1.32 μM for AsO_2^- while respective formation constants were $(2.03 \pm 0.97) \times 10^5$ M^{-1} for $H_2AsO_4^-$

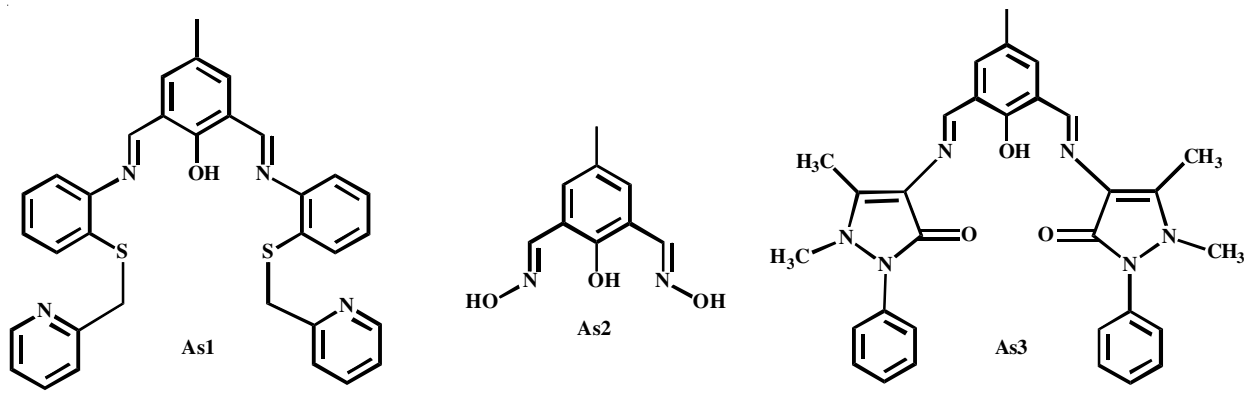

Fig. 4. Arsenicals-selective fluorescent sensors

TABLE-4
CHARACTERISTICS OF ARSENICALS-SELECTIVE FLUORESCENT SENSORS

Sensor used	Medium	$\lambda_{ex}/\lambda_{em}$ (nM)	Detection limit	Binding constant (M^{-1})	Mechanism	Ref.
As1	C_2H_5OH/H_2O (1:99)	440/532	0.001 μM	1.35×10^6	PET, TICT	[47]
As2	H_2O	340/460 ($H_2AsO_4^-$), 340/476 (AsO_2^-)	0.23 μM ($H_2AsO_4^-$), 1.32 μM (AsO_2^-)	$(2.03\pm0.97) \times 10^5$ ($H_2AsO_4^-$), $(2.80\pm0.58) \times 10^4$ (AsO_2^-)	TICT	[48]
As3	DMSO/H_2O (1:9)	438/532	54.91×10^{-9} M	2.5267×10^5	CHEF, PET	[49]

and $(2.80 \pm 0.58) \times 10^4$ M^{-1} for AsO_2^-. The 1:1 stoichiometries of the ensembles formed between sensor-As2, AsO_2^- and $H_2AsO_4^-$ were confirmed by Job's plot and ESI-MS studies. The sensor-As2 can monitor micro molar concentrations of intracellular AsO_2^- and $H_2AsO_4^-$ [48].

Sensor-As3 changes color from colourless solution to faint greenish-yellow colour in the presence of AsO_3^{3-} anions. The fluorescence intensity of sensor-As3 (10 μM, excitation wavelength 438 nm) in 1 mM HEPES buffer (DMSO:H_2O = 1:9, v/v, pH 7.4) at 532 nm was increased about nine-fold (Φ = 0.00228 to Φ = 0.01294) due to the incremental addition of AsO_3^{3-} anions. Based on the fluorescence study, Job's plot revealed the 1:1 stoichiometric ratio of the ensemble formed between sensor-As3 and AsO_3^{3-} anion. The high binding constant value (2.5267×10^5 M^{-1}) obtained from fluorescence titration reflects the strong binding affinity of sensor-As3 towards AsO_3^{3-} anions. The limit of detection was calculated to be 54.91×10^{-9} M. The non-cytotoxic sensor-As3 can detect the intracellular AsO_3^{3-} anions [49].

Pyrophosphate (PPi)-selective fluorescent sensors: Fig. 5 shows the structures of pyrophosphate-selective fluorescent sensors and their characteristic parameters are given in Table-5. In 0.02 M HEPES buffer at pH 7.4, sensor-PPi1 (5 μM, excitation wavelength 440 nm) shows a weak emission at 525 nm, which shifted to a longer wavelength at 552 nm and enhanced by about 8.2-fold after the addition of ~1.0 equiv. of PPi. Based on the fluorescence titration, the stoichiometry between sensor-PPi and PPi anions was found to be 1:1, which was supported by ESI-MS data. Sensor-PPi1 can detect PPi by the naked eye as it changes colour from colourless to pale yellow after the addition of PPi solution. The detection limit of sensor-PPi1 was 155 ppb. When DNA was synthesized by the action of DNA polymerase, stoichiometric amounts of PPi is released from dNTPs. Selective and sensitive fluorescence response of sensor-PPi1 towards PPi enables sensor-PPi, a potential sensor of detection and assessment of DNA in polymerase chain reaction (PCR) products [50].

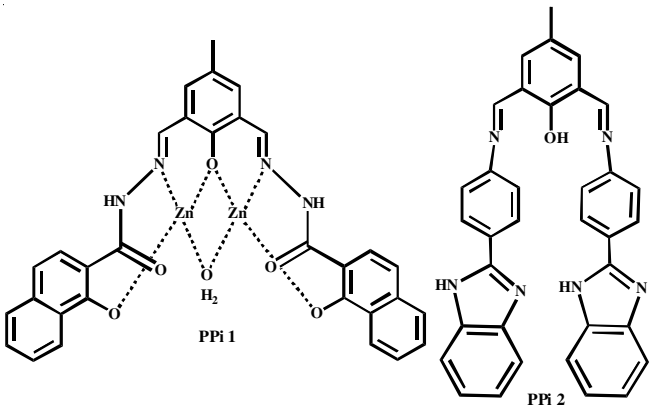

Fig. 5. PPi-selective fluorescent sensors

The aggregation-induced fluorescence intensity of sensor-PPi2 in H_2O (excitation wavelength 430 nm) was increased nearly 17-times more than the sensor-PPi2 alone at 530 nm, upon gradual addition of increasing amounts of PPi. About 10 μM aqueous solution of sensor-PPi2 forms nano-aggregates of average particle size 40-50 nm. The addition of PPi leads to the generation of larger nano-aggregates of average particle size 130-170 nm. This tenet was confirmed by the field emission scanning electron microscope (FESEM) and atomic force microscope (AFM) analysis. The addition of PPi increases the average size of the nano-aggregates, as a consequence, fluorescence intensity was enhanced. The formation of a 1:1 host-guest complex between sensor-PPi2 and PPi was suggested by Job's plot analysis. The apparent binding constant 4.2×10^5 M^{-1} was calculated by the B-H plot. The detection limit of sensor-PPi2 for PPi was evaluated to be 1.67 nM. A distinct visual colour change of sensor-PPi2 solution from colourless to faint yellowish after the addition of PPi encourages naked-eye detection of PPi in water. Sensor-PPi2 and sensor-PPi2-PPi ensemble are non-toxic. Sensor-PPi2 can detect intracellular PPi by imaging studies [51].

pH-Responsive fluorescent sensors: Fig. 6 shows the structures of pH-responsive fluorescent sensors and their characteristic parameters are given in Table-6. Upon excitation at 380 nm, sensor-pH1 (10 μM) in a DMSO-Britton-Robinson buffer (1:9, v/v, pH 7.0) revealed a very weak anthracene unit donor emission at 460 nm and a strong *p*-cresol unit acceptor emission at 537 nm (Φ = 0.31). At pH 5, the anthracene unit donor emission at 460 nm was enhanced and the *p*-cresol unit acceptor emission at 537 nm was suppressed (FRET OFF, Φ = 0.14). At pH 11, the reverse phenomenon was found (FRET ON, Φ = 0.75). At pH 7.0, on excitation at 365 nm, the sensor-pH1′ exhibits emission at 535 nm (Φ = 0.01). The fluorescence intensity was enhanced on moving from neutral to basic pH. Above pH 11, the fluorescence intensity did not increase (Φ = 0.39 at pH 11.0). With a decrease in pH sensor-pH1′ exhibits emission at 600 nm and at pH 2.0, quantum yield was 0.48. Thus, the sensor-pH1′ can detect acidic, basic and neutral pH. Sensor-pH1′ can also detect different pH environments inside the living cell [52].

Upon excitation at 425 nm, sensor-pH2 (10 μM) in Britton-Robinson buffer displays a very weak fluorescence emission at 536 nm in the low pH range and becomes almost non-fluorescent below pH 4.5. The sensor-pH2 exhibits a more than 36-fold fluorescence enhancement within the pH range of 5.0-8.5. This sensor can monitor changes in intracellular H^+ concentration [53].

When excited at 440 nm, the sensor-pH3 in Britton-Robinson buffer displays emission at 528 nm in the low pH range. When

TABLE-5
CHARACTERISTICS OF PPI- SELECTIVE FLUORESCENT SENSORS

Sensor used	Medium	$\lambda_{ex}/\lambda_{em}$ (nM)	Detection limit	Binding constant (M^{-1})	Mechanism	Ref.
PPi1	H_2O	440/552	155 ppb	–	CHEF	[50]
PPi2	H_2O	430/530	1.67 nM	4.2×10^5 M^{-1}	Aggregation induced emission	[51]

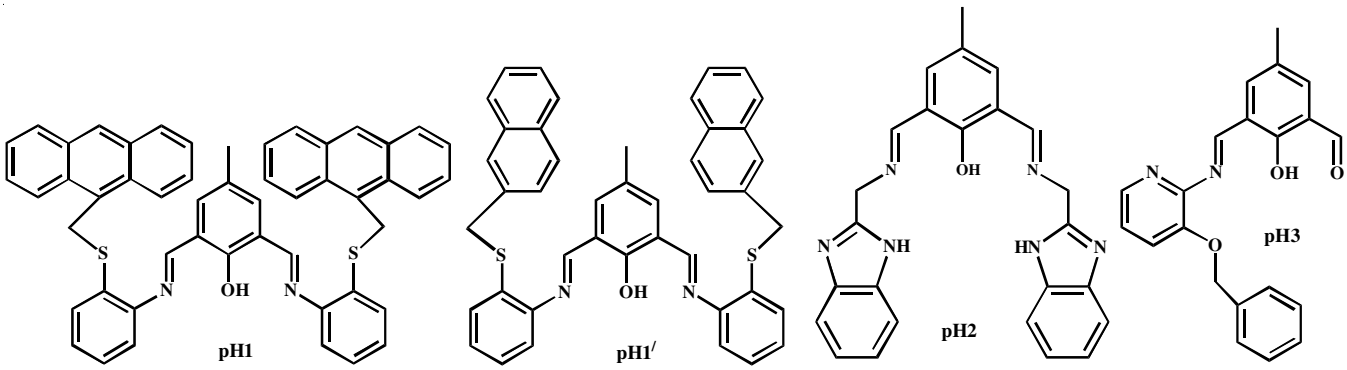

Fig. 6. pH-Responsive fluorescent sensors

TABLE-6
CHARACTERISTICS OF pH-RESPONSIVE FLUORESCENT SENSORS

Sensor used	Medium	$\lambda_{ex}/\lambda_{em}$ (nM)	Detection limit	Binding constant (M^{-1})	Mechanism	Ref.
pH1	DMSO/Britton Robinson buffer (1:9)	380/460, 537 (anthracene), 365/535, 600 (naphthalene)	–	–	FRET	[52]
pH2	Britton-Robinson buffer	425/536	–	–	–	[53]
pH3	Britton-Robinson buffer	440/528, 533	–	–	–	[56]

pH was shifted from 4.2 to 8.3, the sensor-pH3 exhibits 250-fold fluorescence enhancements with a concomitant red shift emission at 533 nm. The increase in fluorescence intensity with the increase in pH was due to the formation of deprotonated sensor anion [54,55]. This sensor can also monitor changes in intracellular pH under biological conditions [56].

Al^{3+}-selective fluorescent sensor: Upon excitation at 460 nm sensor-Al in 0.1 M HEPES-buffered C_2H_5OH:H_2O (4:1, v/v, pH 7.4) exhibited a weak emission at 535 nm ($\Phi = 0.046$) due to the PET from the N-donor site of spirolactam ring to the *p*-cresol moiety. Two emission bands at 509 and 585 nm were obtained after 1 min addition of Al^{3+} (30 μM) to sensor-Al (10 μM). The emission at 509 nm was due to the CHEF between sensor-Al and Al^{3+} with inhibition of PET. The band at 585 nm arised due to Al^{3+}-induced spirolactam ring-opening of rhodamine unit lead to FRET. With increasing time, CHEF emission at 509 nm decreases and FRET emission at 585 nm increases. After 30 min, CHEF emission at 509 nm was diminished and an intense FRET emission at 585 nm was appeared ($\Phi = 0.317$). The limit of detection of sensor-Al for Al^{3+} was found to be 5×10^{-9} M. 2:1 (Al^{3+}:sensor) stoichiometry of the complex between Al^{3+} and sensor-Al was confirmed by Job′s plot. The apparent binding constant 9.1×10^6 M^{-2} was calculated by using the B-H equation. Upon addition of Al^{3+} (60 μM) to the sensor-Al solution (10 μM), a distinct visual colour change from colourless to intense red was observed, which helps naked-eye detection of Al^{3+}. Sensor-Al can detect intracellular Al^{3+} through fluorescence microscope. The sensor-Al also exhibits pH-dependent emission. At acidic pH, the spirolactam ring of rhodamine unit opens and an intense red emission at 585 nm was observed. At basic pH, -OH group of *p*-cresol moiety was deprotonated and green emission at 535 nm was found. Thus, sensor-Al also acts as a pH sensor [57].

Hg^{2+}-selective fluorescent sensor: The fluorescence titration was performed in 50% H_2O/CH_3CN HEPES buffer (20 mM) at pH 7. On excitation at 500 nm, sensor-Hg (10 μM) showed emission at 595 nm in the presence of Hg^{2+} and the fluorescence intensity was > 400-fold enhanced upon addition of 50 equiv. of Hg^{2+}. Based on the fluorescence and UV-vis titration, the detection limit was evaluated to be 10^{-8} M. Sensor-Hg can detect Hg^{2+} ion by the naked-eye as it changes colour from colourless to pink in CH_3CN-HEPES buffer solution after addition of Hg^{2+}. The association constant and stoichiometry of the complex between sensor-Hg and Hg^{2+} were determined 9.21×10^5 M^{-1} and 1:1, respectively. The reversible binding between sensor-Hg and Hg^{2+} was verified through the introduction of I^- anions [58].

Sensor-N_3 (A cationic dinuclear Cu^{2+} complex) proved to be a suitable fluorescent sensor for N_3^- anion. The addition of N_3^- anion to a solution of sensor in H_2O resulted in a colour change from green to dark brown. When excited at 440nm, free sensor-N_3 (50 mM) exhibited a fluorescence at 503 nm ($\Phi = 0.0198$) in aqueous medium. Upon incremental addition of N_3^- (20 mM-7 mM) to the sensor solution (50 mM), the fluorescence maximum underwent a red shift from 503 nm to 528 nm and the fluorescence intensity was increased by six-fold. This fluorescence enhancement was attributed to an increase in the rigidity of hexanuclear complex after N_3^- addition. From the fluorescent titrations, the binding constant and limit of detection of sensor-N_3 with N_3^- in water were calculated to be $2.77 (\pm 0.13) \times 10^3$ M^{-1} L^{-1} and 2.6×10^{-4} g L^{-1}, respectively. From the Job′s plot analysis, it was found that sensor:N_3^- = 1:4. The crystal structure of the complex also supports the ratio [59]. Fig. 7 shows the structures of Al^{3+}, Hg^{2+} and N_3^- selective fluorescent sensors and their characteristic parameters are given in Table-7.

Conclusion

The development of chemosensors for ions has emerged as a significant goal due to their potential applications in environ-

TABLE-7
CHARACTERISTICS OF Al^{3+}, Hg^{2+} AND N_3^--SELECTIVE FLUORESCENT SENSORS

Sensor used	Medium	$\lambda_{ex}/\lambda_{em}$ (nM)	Detection limit	Binding constant (M^{-1})	Mechanism	Ref.
Al	C_2H_5OH/H_2O (4:1)	460/585	5×10^{-9} M	9.1×10^6 M^{-2}	PET, CHEF, FRET	[57]
Hg	CH_3CN/H_2O (1:1)	500/595	10^{-8} M	9.21×10^5 M^{-1}	–	[58]
N_3^-	H_2O	440/528	2.6×10^{-4} g L^{-1}	$2.77\ (\pm 0.13) \times 10^3$	–	[59]

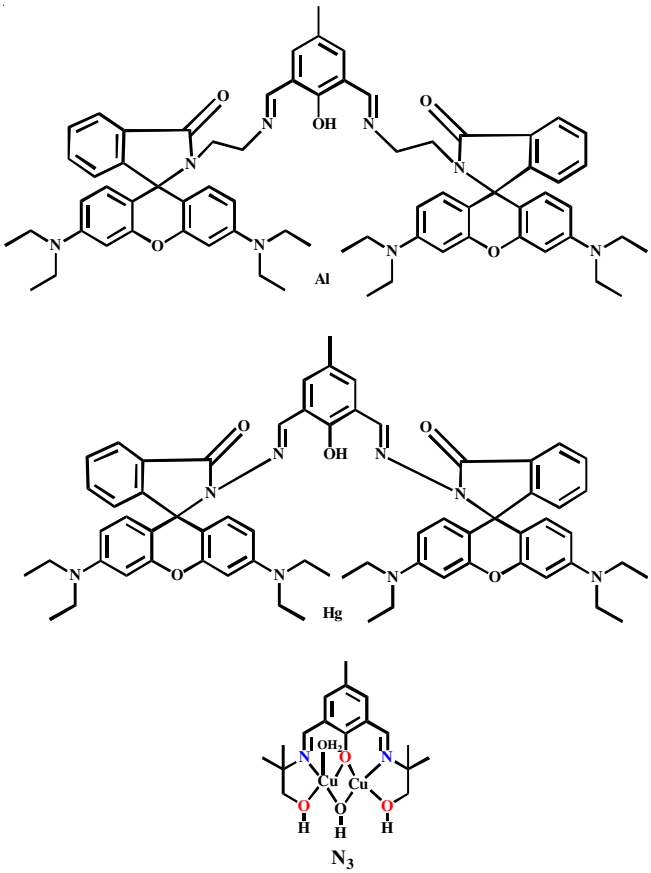

Fig. 7. Al^{3+}, Hg^{2+} and N_3^--Selective fluorescent sensors

mental and biological detection. In this review, the author has focused on 2,6-diformyl-4-methylphenol derived Schiff base fluorescent chemosensors. These chemosensors can be readily prepared by a simple and low-cost Schiff base reaction of 2,6-diformyl-4-methylphenol with the various amines. They detect the metal ions (Zn^{2+}, Al^{3+}, Hg^{2+}, Cd^{2+}, Sn^{2+} and Cu^{2+}) with high sensitivity and selectivity through changes in fluorescence intensity based on CHEF, ICT, FRET, ESIPT, C=N isomerization and PET mechanism. The anions *viz*. HPO_4^{2-}, $H_2PO_4^-$, PO_4^{3-}, AsO_3^{3-}, $H_2AsO_4^-$, AsO_2^-, PPi, I^-, F^- and N_3^- anions were also detected through intermolecular hydrogen bonding (between sensor and anion) based on TICT, PET, CHEF, ESIPT and aggregation induced Emission mechanisms. Selectivity and sensitivity for these metal ions and anions were achieved by introducing various amines to core fluorophore 2,6-diformyl-4-methylphenol.

CONFLICT OF INTEREST

The authors declare that there is no conflict of interests regarding the publication of this article.

REFERENCES

1. A.W. Czarnik, *Acc. Chem. Res.*, **27**, 302 (1994); https://doi.org/10.1021/ar00046a003
2. A.T. Wright and E.V. Anslyn, *Chem. Soc. Rev.*, **35**, 14 (2006); https://doi.org/10.1039/B505518K
3. V. Amendola and L. Fabbrizzi, *Chem. Commun.*, 513 (2009); https://doi.org/10.1039/b808264m
4. L. Prodi, *New J. Chem.*, **29**, 20 (2005); https://doi.org/10.1039/b411758a
5. J. Yoon, S.K. Kim, N.J. Singh and K.S. Kim, *Chem. Soc. Rev.*, **35**, 355 (2006); https://doi.org/10.1039/b513733k
6. A.W. Czarnik, *Instrumen. Sci. Technol.*, **22**, 405 (1994); https://doi.org/10.1080/10739149408001201
7. A.P.S. Gonzáles, M.A. Firmino, C.S. Nomura, F.R.P. Rocha, P.V. Oliveira and I. Gaubeur, *Anal. Chim. Acta*, **636**, 198 (2009); https://doi.org/10.1016/j.aca.2009.01.047
8. J.S. Becker, A. Matusch, C. Depboylu, J. Dobrowolska and M.V. Zoriy, *Anal. Chem.*, **79**, 6074 (2007); https://doi.org/10.1021/ac0700528
9. Y. Liu, P. Liang and L. Guo, *Talanta*, **68**, 25 (2005); https://doi.org/10.1016/j.talanta.2005.04.035
10. A.A. Ensafi, T. Khayamian, A. Benvidi and E. Mirmomtaz, *Anal. Chim. Acta*, **561**, 225 (2006); https://doi.org/10.1016/j.aca.2006.01.015
11. Y.H. Hung, A.I. Bush and R.A. Cherny, *J. Biol. Inorg. Chem.*, **15**, 61 (2010); https://doi.org/10.1007/s00775-009-0600-y
12. B.-C. Yin, B.-C. Ye, W. Tan, H. Wang and C.-C. Xie, *J. Am. Chem. Soc.*, **131**, 14624 (2009); https://doi.org/10.1021/ja9062426
13. T.-W. Lin and S.-D. Huang, *Anal. Chem.*, **73**, 4319 (2001); https://doi.org/10.1021/ac010319h
14. G. Sivaraman, T. Anand and D. Chellappa, *RSC Adv.*, **3**, 17029 (2013); https://doi.org/10.1039/c3ra42109k
15. M. Suresh, A. Ghosh and A. Das, *Chem. Commun.*, 3906 (2008); https://doi.org/10.1039/b807290f
16. V. Bhalla, V. Vij, M. Kumar, P.R. Sharma and T. Kaur, *Org. Lett.*, **14**, 1012 (2012); https://doi.org/10.1021/ol203339c
17. A. Kumar, A. Kumar and D.S. Pandey, *Dalton Trans.*, **45**, 8475 (2016); https://doi.org/10.1039/C6DT00747C
18. P.S. Hariharan and S.P. Anthony, *Anal. Chim. Acta*, **848**, 74 (2014); https://doi.org/10.1016/j.aca.2014.07.042
19. K.-L. Han and G.-J. Zhao, Hydrogen Bonding and Transfer in the Excited State, Wiley (2010).
20. A. Gupta and N. Kumar, *RSC Adv.*, **6**, 106413 (2016); https://doi.org/10.1039/C6RA23682K
21. M. Formica, V. Fusi, L. Giorgi and M. Micheloni, *Coord. Chem. Rev.*, **256**, 170 (2012); https://doi.org/10.1016/j.ccr.2011.09.010
22. J. Wu, W. Liu, J. Ge, H. Zhang and P. Wang, *Chem. Soc. Rev.*, **40**, 3483 (2011); https://doi.org/10.1039/c0cs00224k
23. S. Anbu, R. Ravishankaran, M.F.C. Guedes da Silva, A.A. Karande and A.J.L. Pombeiro, *Inorg. Chem.*, **53**, 6655 (2014); https://doi.org/10.1021/ic500313m
24. M. Sarkar, S. Banthia and A. Samanta, *Tetrahedron Lett.*, **47**, 7575 (2006); https://doi.org/10.1016/j.tetlet.2006.08.091
25. P. Roy, K. Dhara, M. Manassero, J. Ratha and P. Banerjee, *Inorg. Chem.*, **46**, 6405 (2007); https://doi.org/10.1021/ic700420w

26. K. Sarkar, K. Dhara, M. Nandi, P. Roy, A. Bhaumik and P. Banerjee, *Adv. Funct. Mater.*, **19**, 223 (2009); https://doi.org/10.1002/adfm.200800888
27. A. Jana, P.K. Sukul, S.K. Mandal, S. Konar, S. Ray, K. Das, J.A. Golen, A.L. Rheingold, S. Mondal, T.K. Mondal, A.R. Khuda-Bukhsh and S.K. Kar, *Analyst*, **139**, 495 (2014); https://doi.org/10.1039/C3AN01750H
28. C. Patra, A.K. Bhanja, C. Sen, D. Ojha, D. Chattopadhyay, A. Mahapatra and C. Sinha, *RSC Adv.*, **6**, 53378 (2016); https://doi.org/10.1039/C6RA07089B
29. A. Jana, B. Das, S.K. Mandal, S. Mabhai, A.R. Khuda-Bukhsh and S. Dey, *New J. Chem.*, **40**, 5976 (2016); https://doi.org/10.1039/C6NJ00234J
30. T.A. Khan, M. Sheoran, V.N. Raj M.S. Jain, D. Gupta and S.G. Naik, *Spectrochim. Acta A Mol. Biomol. Spectrosc.*, **189**, 176 (2018); https://doi.org/10.1016/j.saa.2017.08.017
31. U.C. Saha, B. Chattopadhyay, K. Dhara, S.K. Mandal, S. Sarkar, A.R. Khuda-Bukhsh, M. Mukherjee, M. Helliwell and P. Chattopadhyay, *Inorg. Chem.*, **50**, 1213 (2011); https://doi.org/10.1021/ic1015252
32. P. Roy, K. Dhara, M. Manassero and P. Banerjee, *Inorg. Chim. Acta*, **362**, 2927 (2009); https://doi.org/10.1016/j.ica.2009.01.023
33. K. Dhara, S. Karan, J. Ratha, P. Roy, G. Chandra, M. Manassero, B. Mallik and P. Banerjee, *Chem. Asian J.*, **2**, 1091 (2007); https://doi.org/10.1002/asia.200700152
34. A.K. Bhanja, C. Patra, S. Mondal, S. Mishra, K.D. Saha and C. Sinha, *Sens. Actuators B Chem.*, **252**, 257 (2017); https://doi.org/10.1016/j.snb.2017.05.178
35. S. Lohar, S. Pal, M. Mukherjee, A. Maji, P. Chattopadhyay and N. Demitri, *RSC Adv.*, **7**, 25528 (2017); https://doi.org/10.1039/C7RA02175E
36. R. Purkait, A.D. Mahapatra, D. Chattopadhyay and C. Sinha, *Spectrochim. Acta A Mol. Biomol. Spectrosc.*, **207**, 164 (2019); https://doi.org/10.1016/j.saa.2018.09.019
37. R. Purkait, S. Maity and C. Sinha, *New J. Chem.*, **42**, 6236 (2018); https://doi.org/10.1039/C7NJ04533F
38. S. Lohar, A. Sengupta, A. Chattopadhyay, J.S. Matalobos and D. Das, *Eur. J. Inorg. Chem.*, **2014**, 5675 (2014); https://doi.org/10.1002/ejic.201402702
39. S. Nandi and D. Das, *ACS Sens.*, **1**, 81 (2016); https://doi.org/10.1021/acssensors.5b00035
40. B.K. Datta, D. Thiyagarajan, A. Ramesh and G. Das, *Dalton Trans.*, **44**, 13093 (2015); https://doi.org/10.1039/C5DT01468A
41. R. Alam, T. Mistri, R. Bhowmick, A. Katarkar, K. Chaudhuri and M. Ali, *RSC Adv.*, **5**, 53940 (2015); https://doi.org/10.1039/C5RA08024J
42. R. Purkait, S. Dey and C. Sinha, *New J. Chem.*, **42**, 16653 (2018); https://doi.org/10.1039/C8NJ03165G
43. S. Adhikari, S. Mandal, A. Ghosh, S. Guria and D. Das, *Dalton Trans.*, **44**, 14388 (2015); https://doi.org/10.1039/C5DT02146D
44. C. Kar, M.D. Adhikari, B.K. Datta, A. Ramesh and G. Das, *Sens. Actuators B Chem.*, **188**, 1132 (2013); https://doi.org/10.1016/j.snb.2013.08.005
45. B. Naskar, R. Modak, D.K. Maiti, A. Bauzá, A. Frontera, P.K. Maiti, S. Mandal and S. Goswami, *RSC Adv.*, **7**, 11312 (2017); https://doi.org/10.1039/C6RA27017D
46. V. Chandrasekhar, S. Das, R. Yadav, S. Hossain, G. Subramaniam, R. Parihar and P. Sen, *Inorg. Chem.*, **51**, 8664 (2012); https://doi.org/10.1021/ic301399a
47. A. Banerjee, A. Sahana, S. Lohar, S. Panja, S.K. Mukhopadhyay and D. Das, *RSC Adv.*, **4**, 3887 (2014); https://doi.org/10.1039/C3RA45362F
48. A.S.M. Islam, R. Alam, A. Katarkar, K. Chaudhuri and M. Ali, *Analyst*, **140**, 2979 (2015); https://doi.org/10.1039/C5AN00236B
49. S. Lohar, S. Pal, B. Sen, M. Mukherjee, S. Banerjee and P. Chattopadhyay, *Anal. Chem.*, **86**, 11357 (2014); https://doi.org/10.1021/ac503255f
50. S. Anbu, S. Kamalraj, C. Jayabaskaran and P.S. Mukherjee, *Inorg. Chem.*, **52**, 8294 (2013); https://doi.org/10.1021/ic4011696
51. A. Gogoi, S. Mukherjee, A. Ramesh and G. Das, *Anal. Chem.*, **87**, 6974 (2015); https://doi.org/10.1021/acs.analchem.5b01746
52. A. Banerjee, A. Sahana, S. Lohar, B. Sarkar, S.K. Mukhopadhyay and D. Das, *RSC Adv.*, **3**, 14397 (2013); https://doi.org/10.1039/C3RA41591K
53. U.C. Saha, S.K. Mandal, S. Pal, A.R. Khuda-Bukhsh, P. Chattopadhyay and K. Dhara, *Biochem. Mol. Biol. Lett.*, **1**, 065 (2015).
54. M. Mukhopadhyay, D. Banerjee and S. Mukherjee, *J. Phys. Chem. A*, **110**, 12743 (2006); https://doi.org/10.1021/jp063724r
55. S. Mitra and S. Mukherjee, *J. Lumin.*, **118**, 1 (2006); https://doi.org/10.1016/j.jlumin.2005.04.014
56. U.C. Saha, K. Dhara, B. Chattopadhyay, S.K. Mandal, S. Mondal, S. Sen, M. Mukherjee, S. van Smaalen and P. Chattopadhyay, *Org. Lett.*, **13**, 4510 (2011); https://doi.org/10.1021/ol201652r
57. A. Sahana, A. Banerjee, S. Lohar, B. Sarkar, S.K. Mukhopadhyay and D. Das, *Inorg. Chem.*, **52**, 3627 (2013); https://doi.org/10.1021/ic3019953
58. Z. Dong, X. Tian, Y. Chen, J. Hou, Y. Guo, J. Sun and J. Ma, *Dyes Pigments*, **97**, 324 (2013); https://doi.org/10.1016/j.dyepig.2013.01.002
59. K. Dhara, U.C. Saha, A. Dan, M. Manassero, P. Chattopadhyay and S. Sarkar, *Chem. Commun.*, **46**, 1754 (2010); https://doi.org/10.1039/b919937c